Research Article | Open Access

Iontronics

Li *et al. Iontronics* **2026**, *2*, 35 **DOI:**10.20517/iontronics.2026.28

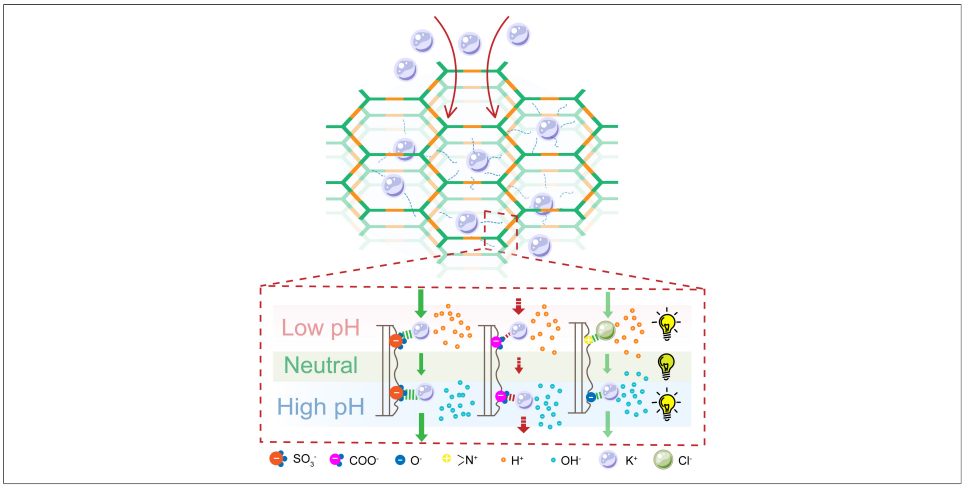
pH-gated ion transport in covalent organic framework membranes functionalized with oxygen-containing groups

Ping Li, Jieyu Zhang, Liuna Luo, Mingshuai Yang, Anran Xia, Yuanyuan Niu, Bing Sun*

Keywords:
Covalent organic framework membranes, pH-gated ion transport, nanofluidic ion gating, surface charge regulation, functional group engineering

Citation: Li, P.; Zhang, J.; Luo, L.; Yang, M.; Xia, A.; Niu, Y.; Sun, B. pH-gated ion transport in covalent organic framework membranes functionalized with oxygen-containing groups. *Iontronics* **2026**, *2*, 35. https://dx.doi.org/10.20517/iontronics.2026.28

Received: 4 Jul 2026
First Decision: 13 Aug 2026
Revised: 8 Sep 2026
Accepted: 8 Oct 2026
Published: 4 Nov 2026



Abstract

Covalent organic framework (COF) membranes with pH-gated ion transport hold promise for smart nanofluidic devices, yet the regulatory mechanisms of different oxygen-containing functional groups remain poorly understood. Herein, we systematically investigate the pH-dependent ionic conductance of TpPa-R COF membranes (R = -SO_3H, -COOH, -OH) across pH 3 to 11.5 using unmodified TpPa as a reference. All membranes exhibit nanofluidic transport with a U-shaped conductance profile as a function of pH. The neutral-pH conductance is governed by the effective surface charge density that drives counterion enrichment. Among the three modifications, the TpPa-SO_3H membrane displays the broadest pH response and the highest conductance at both acidic and alkaline extremes. Notably, the TpPa-COOH membrane shows unexpectedly lower conductance than TpPa-OH at pH ≥ 5, which we attribute to hydration screening that reduces the effective charge of the carboxylate groups, whereas deprotonation of the phenol groups in TpPa-OH enhances effective surface charge density and conductance at high pH. All membranes demonstrate reversible pH-switching over the tested range. This work provides a molecular-level design rationale for tailoring pH-gating performance in COF membranes and a foundation for developing tunable ion-transport devices with predictable pH responsiveness.

Check for updates

School of Science, China University of Geosciences (Beijing), Beijing 100083, China.

***Correspondence to:** Dr. Bing Sun, School of Science, China University of Geosciences (Beijing), Beijing 100083, China. E-mail: sunbing@cugb.edu.cn

INTRODUCTION

Biological ion channels achieve precise ion transport through specialized structural motifs. Their dynamic adaptation through conformational changes and structural plasticity supports physiological functions ranging from neuronal signaling to cellular homeostasis[1-3]. Among these regulatory mechanisms, pH-responsive ion transport is especially prevalent. It exploits the chemical simplicity of protonation/deprotonation to mediate processes such as synaptic transmission and sensory transduction[4,5]. This protonation/deprotonation provides a clean, reversible, and byproduct-free chemical switch, which has inspired extensive efforts to replicate pH-gated functions in synthetic nanofluidic systems[6-8]. In artificial nanofluidic systems, pH-gated ion transport is typically achieved by introducing ionizable functional groups onto channel walls, where nanoconfinement allows the surface charge density to govern the electrostatic interactions[9,10]. This design principle has been explored across various material platforms for biosensing and biomimetic iontronic applications that require switchable ion gating[11-13]. Among these ionizable groups, oxygen-containing functionalities are common and synthetically accessible, yet their differential roles in pH-gated ion transport under nanoconfinement have not been systematically compared within a common framework.

A systematic comparison of oxygen-containing functional groups requires a platform in which they can be varied within an identical framework. Covalent organic frameworks (COFs) meet this requirement. Their reticular chemistry enables diverse functional groups to be incorporated into a common framework, and their ordered nanochannels with pore sizes of sub-2 nm to 4 nm provide a well-defined environment for investigating nanoconfined ion transport[14,15]. At these length scales, the pore dimensions are comparable to the Debye length, so that surface charge and channel size jointly govern ion transport rather than bulk diffusion alone[16,17]. Pore-wall chemistry in COFs has been shown to effectively modulate ion transport[18,19], and the pH responsiveness of COF membranes generally arises from pH-responsive functionalities within the pores.

Several strategies have been developed to engineer pH-responsive COF membranes. Direct chemical functionalization is exemplified by COF-DT membranes, in which imine linkages and phenolic hydroxyl groups enable pH-gated ion transport with an ON/OFF ratio of ~ 100[13], and by carboxyl-functionalized TpPa-COOH membranes that exhibit pH-dependent Na^+/K^+ selectivity switching[20]. Channel geometry engineering instead introduces pH-responsive molecules that modulate the effective dimensions of the nanochannels. Hourglass-shaped COF-CDN membranes with amino-cyclodextrin at the channel mouths endow the hetero-nanochannels with pH-responsive ability, allowing dynamic regulation of pore size and surface charge[21]. In dopamine-mediated channel engineering, pH-sensitive dopamine acts as a molecular spacer that modulates the effective pore size, enabling pH-switchable K^+/Li^+ selectivity up to 18.7[22]. Biomimetic approaches draw inspiration from biological ion channels that regulate ion selectivity and conductance through protonation/deprotonation of specific residues. Cysteine-functionalized COF-Cys membranes, for example, achieve pH-stimulated switching between K^+- and Na^+-selective states and reversible membrane potential polarity[23]. These studies demonstrate the versatility of COFs for pH-responsive gating and highlight the growing interest in smart responsive functions such as switchable membrane potential.

The reported COF membranes involve different frameworks, pore architectures, and measurement conditions, which complicates the isolation of the functional group's role. The TpPa platform offers a robust β-ketoenamine-linked framework with high chemical stability and functionalization sites on the diamine linker, allowing different oxygen-containing groups to be introduced without altering the framework topology. Within the TpPa family, TpPa-SO_3H has been studied for proton conduction[24,25], molecular sieving[26], and monovalent cation separation[27], while TpPa-COOH has been investigated for pH-dependent

ion selectivity in capacitive deionization[20]. However, a systematic comparison of different oxygen-containing groups within the same TpPa framework under identical conditions has not been conducted. The fundamental parameter beyond pKa that governs ion transport in nanoconfined COF channels remains to be elucidated.

Herein, we investigate pH-gated ion transport through TpPa-R COF membranes (R = -OH, -COOH, or -SO_3H groups, Figure 1A) constructed from 1,3,5-triformylphloroglucinol (Tp) and 1,4-phenylenediamine (Pa) derivatives (Pa-R). Unmodified TpPa serves as a reference to isolate the role of pore-wall functional groups. All membranes exhibit surface-charge-governed transport at low ionic strength, with a U-shaped pH-dependent conductance governed by the effective surface charge density rather than acid strength alone. TpPa-SO_3H displays the broadest pH response and the higher conductance at both acidic and alkaline extremes, consistent with its fully dissociated sulfonate groups. In contrast, TpPa-COOH shows unexpectedly lower conductance than TpPa-OH at pH ≥ 5, attributed to hydration screening of the carboxylate groups that reduces the effective charge density. All four membranes exhibit reversible pH switching over pH 3-11.5, with TpPa-COOH reaching ON/OFF ratios of 113 and 114 for acidic-neutral and alkaline-neutral switching, respectively. Under asymmetric pH conditions, the membranes also show reversible membrane potential polarity switching, enabling dynamic control over ion selectivity. These findings provide molecular-level design rules for functional-group engineering of pH-gating COF membranes and suggest their potential for biomimetic iontronic applications.

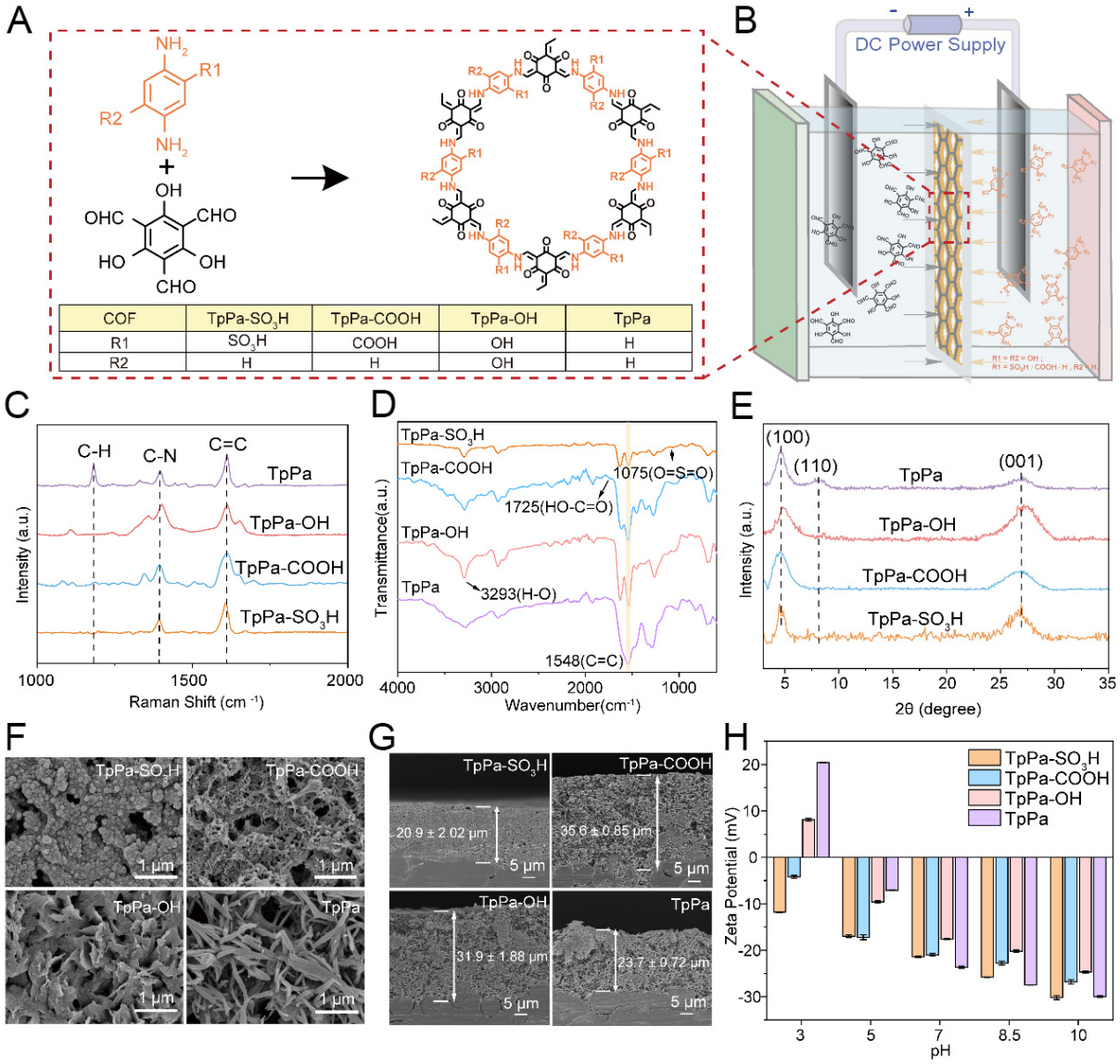
EXPERIMENTAL

Preparation of TpPa-R COF membranes

TpPa and TpPa-R COF membranes were synthesized at room temperature by electric-field-assisted interfacial polymerization on an NL-66 substrate, adapted from a previously reported procedure[28]. The reaction used 1,3,5-triformylphloroglucinol (Tp) and either 1,4-phenylenediamine (Pa) or oxygen-containing Pa-R derivatives (R = -OH, -COOH, or -SO_3H, specifically, 2,5-diaminobenzene-1,4-diol dihydrochloride, 2,5-diaminobenzoic acid, and 2,5-diaminobenzenesulfonic acid, respectively; Figure 1A). Tp, Pa, methanol, and *n*-octanoic acid were obtained from InnoChem (Beijing). 2,5-diaminobenzene-1,4-diol dihydrochloride [Pa-$(OH)_2$], 2,5-diaminobenzoic acid (Pa-COOH), and 2,5-diaminobenzenesulfonic acid (Pa-SO_3H) were purchased from Shanghai Macklin Biochemical Co., Ltd. In a typical procedure, Tp (0.1 mmol) was dissolved in methanol (45 mL) to form the aldehyde monomer solution. The amine solution was prepared by dissolving Pa or Pa-R (0.15 mmol) in methanol (45 mL) with 1 mL of *n*-octanoic acid under ultrasonication for 5 min. As shown in Figure 1B, an H-shaped electrochemical cell with a channel diameter of 1.5 cm was assembled with an NL-66 substrate (diameter 2.5 cm, 0.22 μm pore size, supplied by Haining Delv New Material Technology Co., Ltd) clamped between its two compartments; the aldehyde and amine solutions (45 mL each) were slowly added into the two compartments, respectively. Two Pt foil electrodes (1 cm × 2 cm) were placed in parallel, one in each compartment, with the anode in the amine solution and the cathode in the aldehyde solution. A direct current (DC) voltage of 3 V was applied between the electrodes to induce the synthesis. Under the applied electric field, charged amine monomers migrated across the NL-66 substrate from the anodic compartment (amine side) toward the cathodic compartment (aldehyde side), initiating the interfacial polycondensation with Tp monomers via Schiff-base reaction and keto-enol tautomerism. This process resulted in the formation and growth of β-ketoenamine-linked TpPa and TpPa-R membranes on the surface of the NL-66 substrate. After 8 h of reaction, the resulting membranes were rinsed successively with acetone, ethanol, and water and then stored in deionized water.

Ionic conductance measurements

Ionic conductance was measured at room temperature using a Keithley 2614B source meter and an H-shaped electrochemical cell. The NL-66-supported TpPa or TpPa-R membrane (effective area of 1.77 cm^2) was clamped between the two compartments of the cell, and each compartment was filled with 15 mL of KCl



COF	TpPa-SO_3H	TpPa-COOH	TpPa-OH	TpPa
R1	SO_3H	COOH	OH	H
R2	H	H	OH	H

Figure 1. (A) Chemical structures of TpPa and TpPa-R; (B) Schematic diagram of the electric-field-assisted interfacial polymerization process; (C) Raman spectra, (D) FTIR spectra, and (E) XRD patterns of the TpPa and TpPa-R membranes; (F) Top-view and (G) cross-sectional SEM images; (H) Zeta (ζ) potentials of TpPa and TpPa-R membranes as a function of pH from 3 to 10. Membrane thicknesses in panel (G) are given as mean ± standard deviation, and error bars in panel (H) represent the standard deviation obtained from three independent measurements for each sample. COF: Covalent organic framework; DC: Direct current; FTIR: Fourier transform infrared; XRD: X-ray diffraction; SEM: scanning electron microscopy.

solution. For each of the four membranes, measurements were performed over a full matrix of conditions: KCl concentrations from 10^{-7} M to 10^{-1} M in tenfold serial dilutions, and pH values of 3, 5, 7, 9.5, and 11.5. A pair of Ag/AgCl electrodes was used to record the transmembrane ionic current. Linear voltage sweeps were applied from -1.5 to +1.5 V at a scan rate of 10 mV/s, and the steady-state I-V curves were obtained. Ionic conductance was then calculated from the slope of each curve. All ionic conductance measurements were performed in triplicate for each membrane under each set of conditions to ensure reproducibility. Cation transference numbers (t_+) were measured and calculated as described in the Supplementary Materials. For each membrane, measurements were performed five times, and the mean t_+ value and the standard deviation were calculated from these measurements.

Membrane potential measurements

The pH-gradient membrane potential was measured at room temperature using a CHI660E electrochemical workstation and the same H-shaped electrochemical cell setup used for the conductance measurements, with the COF membrane clamped between the two compartments. Both compartments were filled with 10^{-2} M KCl solutions; the pH was maintained at 7 on one side and switched between 3 and 11.5 on the other. A pair of Ag/AgCl electrodes was used to monitor the open-circuit potential (OCP) in real time. In a typical pH-switching cycle, the OCP was first recorded for 300 s with the test side at pH 3. The test side solution was then removed, and the compartment was rinsed sequentially with deionized water and 10^{-2} M KCl solution at pH 11.5 (two or three times each), before being refilled with fresh 10^{-2} M KCl at pH 11.5. The OCP was then recorded for another 300 s. The same procedure was applied for the reverse switch (from pH 11.5 to pH 3). This pH-switching protocol between 3 and 11.5 was repeated for three consecutive cycles.

General characterizations

Powder X-ray diffraction (PXRD) patterns were recorded at room temperature on a PANalytical Empyrean diffractometer using Cu Kα radiation (λ = 1.5416 Å) at 40 kV and 40 mA, with a scanning range of 2.5° to 35° and a speed of 2° min^{-1}. Raman spectra were acquired on a Thermo Scientific DXR Raman spectrometer over the range of 1,000-2,000 cm^{-1} with a 633 nm laser. Fourier transform infrared (FTIR) spectra were recorded on a Thermo Scientific Nicolet spectrometer equipped with a Smart iTX-Diamond ATR accessory at room temperature, with 64 scans per spectrum. Scanning electron microscopy (SEM) images were obtained on a Hitachi SU8010 field-emission SEM to examine membrane surface morphology and cross-sectional structure. Before imaging, samples were sputter-coated with a thin layer of gold to improve conductivity. The top-view and cross-sectional images were acquired at an accelerating voltage of 5.0 kV and a working distance of approximately 8 mm. Surface ζ potential as a function of solution pH was measured on an Anton Paar SurPASS solid surface ζ potential analyzer using 10^{-3} M KCl at room temperature, with the pH adjusted to 3, 5, 7, 8.5, and 10.

RESULTS AND DISCUSSION

Characterization of TpPa and TpPa-R membranes

The structures of the synthesized membranes were characterized by Raman spectroscopy, FTIR, and XRD. Raman spectra are consistent with the formation of the β-ketoenamine framework in all membranes [Figure 1C], with characteristic bands at ~1,180, 1,395, and 1,608 cm^{-1} assigned to C-H, C-N, and aromatic C=C vibrations, respectively[29]. Slight peak shifts and broadening in the TpPa-R derivatives may reflect the incorporation of the intended functional groups. FTIR spectra further support the proposed chemical structures [Figure 1D]. All four membranes exhibit the characteristic C=C absorption of the β-ketoenamine framework at ~ 1,537-1,548 cm^{-1}. For the functionalized derivatives, the spectrum of TpPa-OH shows a distinct O-H stretching band at ~ 3,293 cm^{-1}, whereas the diagnostic signals for sulfonic (S=O at ~1,075 cm^{-1}) and carboxyl (C=O at ~1,725 cm^{-1}) groups are relatively weak but discernible[30], likely because of the lower oscillator strength of these vibrations or their involvement in hydrogen bonding.

XRD patterns of the membrane samples [Figure 1E] show three characteristic peaks at 4.6°, 8.0°, and 27.0°, assignable to the (100), (110), and (001) planes of the hexagonal β-ketoenamine COFs, consistent with an eclipsed stacking configuration [Supplementary Figure 1][31]. The slight shift of the TpPa-OH peaks to higher 2θ angles suggests tighter layer packing, possibly arising from strong intermolecular hydrogen bonding between the hydroxyl groups. In contrast, TpPa-COOH and TpPa-SO_3H show negligible shifts, indicating that these functional groups do not significantly alter the interlayer spacing and that the framework remains essentially unchanged after functionalization. The pore sizes derived from the structural models are comparable among the four membranes, ranging from approximately 1.5 to 1.8 nm [Supplementary Table 1]. These findings provide a structurally consistent platform for isolating the effects of pore-wall chemistry

on ion transport behavior.

SEM images revealed substituent-dependent morphological variations among the four membranes [Figure 1F and G]. The unmodified TpPa membrane displays band-like aggregates with individual diameters of approximately 680 nm, forming a relatively dense layer on the substrate with an average thickness of 23.7 ± 0.72 μm. Interstitial voids are visible among the aggregates. TpPa-OH exhibits a looser, sheet-like surface morphology and a densely stacked cross-section with a thickness of 31.9 ± 1.88 μm. TpPa-COOH consists of entangled fibrils and has a larger thickness of 35.6 ± 0.85 μm. TpPa-SO_3H presents particle-aggregated porous structures with a dense and smooth cross-section of 20.9 ± 2.02 μm. Despite these morphological differences, all membranes adhere well to the substrate and remain structurally intact, with no visible cracks or delamination. Although thickness variations may influence the absolute conductance values, the distinct pH-gating behaviors discussed below arise primarily from differences in surface charge chemistry rather than morphological features.

Zeta (ζ) potential measurements revealed clear substituent-dependent surface charge behavior for all four membranes (Figure 1H; values with standard deviations are provided in Supplementary Table 2). For all membranes, the ζ potential decreases monotonically with increasing pH, consistent with progressive deprotonation of framework-bound ionizable groups. However, these trends vary in detail with the functional group. TpPa-SO_3H, bearing strongly acidic sulfonate groups (pKa < 0), remains negatively charged across the entire pH range, with a high charge density that increases from -11.8 mV at pH 3 to -30.2 mV at pH 10. TpPa-COOH shows a sharp transition between pH 3 and pH 5, shifting from near-neutral (-4.2 mV) to strongly negative (-17.2 mV), consistent with the deprotonation of carboxyl groups (pKa ≈ 4-5). The ζ potential decreases further, albeit more gradually above pH 7, reaching -26.8 mV at pH 10. In contrast, TpPa-OH and unmodified TpPa are positively charged at pH 3 (+8.1 and +20.4 mV, respectively), indicating protonated imine linkages or residual amine groups, and both become negatively charged above pH 5. Particularly, unmodified TpPa becomes more negative than TpPa-OH at pH ≥ 7 (-23.7 *vs.* -17.6 mV at pH 7; -30.0 *vs.* -24.7 mV at pH 10), suggesting additional deprotonatable sites on the unsubstituted framework. The pH at which the ζ potential crosses zero, together with the magnitude of the negative charge at high pH, reflects the acid strength of the functional groups. These charge profiles, primarily governed by the pKa of each modifier, provide the molecular basis for the pH-gated ion transport behavior discussed below.

Surface-charge-governed ion transport at neutral pH

Ion transport through the four TpPa-based membranes was investigated in symmetric KCl solutions (10^{-7} to 10^{-1} M) at pH 7. Representative I-V curves at 10^{-6} M [Figure 2A] and full concentration-dependent I-V data [Supplementary Figure 2] show linear responses for all membranes, indicating ohmic transport behavior and allowing conductance to be extracted from the slope of each curve. The concentration-dependent conductance profiles [Figure 2B] show a transition from bulk-dominated to surface-charge-governed transport as the salt concentration decreases. In the high-concentration regime (above 10^{-5} M), conductance decreases approximately linearly with dilution for all four membranes. Here, the abundant bulk ions effectively screen the surface charges of the nanochannels and govern ion transport. At 10^{-1} M KCl, the three functionalized membranes exhibit higher conductance than TpPa. As the concentration decreases to 10^{-2}-10^{-4} M, the conductance of TpPa-COOH, TpPa-OH, and TpPa converges to comparable values, all remaining lower than that of TpPa-SO_3H.

Upon dilution to 10^{-5} M, the conductance across the four membranes decreases to 0.91-2.49 μS [Supplementary Table 3], marking a departure from the bulk-dominated linear regime. The Debye length here approaches the nanochannel dimensions, and bulk ions become depleted within the pores[32]. Transport is now governed by the negatively charged pore walls, which selectively enrich cations and exclude anions,

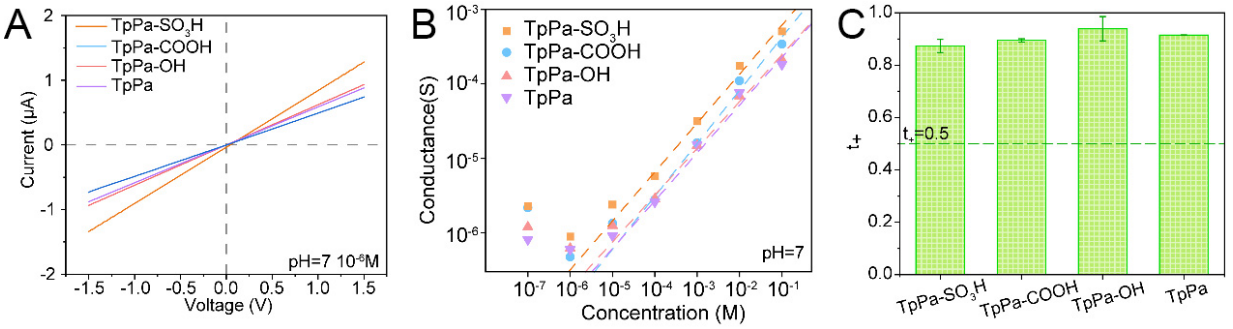


Figure 2. (A) Representative I-V curves of the four membranes in 10^{-6} M KCl at pH 7; (B) Ionic conductance as a function of KCl concentration (10^{-7} to 10^{-1} M) at pH 7; (C) Cation transference numbers (t_+) measured under a tenfold KCl concentration gradient (10^{-3} M *vs.* 10^{-2} M) at pH 7. Error bars in (C) represent the standard deviation obtained from five independent measurements for each sample.

maintaining a counterion concentration that far exceeds the bulk value. At 10^{-6} M, the surface-charge-governed regime yields a conductance ranking of TpPa-SO_3H > TpPa ≈ TpPa-OH > TpPa-COOH, which does not follow the order of ζ potentials measured at pH 7. For instance, TpPa and TpPa-SO_3H have comparable ζ potentials (-23.7 and -21.4 mV), yet TpPa-SO_3H shows higher conductance. Conversely, TpPa-COOH demonstrates a more negative ζ potential than TpPa-OH (-21.0 *vs.* -17.6 mV) but exhibits lower conductance. Upon further dilution to 10^{-7} M, the ranking shifts to TpPa-SO_3H ≈ TpPa-COOH > TpPa-OH > TpPa. These deviations from the ζ potential trend indicate that net surface charge alone does not govern ion transport. The chemical identity of the charged groups and, under extreme dilution, the contribution of hydronium ions must also be considered.

Cation transference numbers (t_+) measured under a tenfold KCl concentration gradient [Figure 2C] exceed 0.8 for all four membranes, confirming strong monovalent cation selectivity. The TpPa-OH membrane reaches the highest value of 0.94 ± 0.04, which is comparable to that of a reported 3D sulfonated COF membrane (t_+ = 0.976)[33]. These results provide a baseline at pH 7 for the pH-dependent behavior examined in the following section, where protonation and deprotonation of the functional groups systematically modulate the surface charge and, in turn, the ion transport properties.

pH-gated ion transport in TpPa-based COF membranes

To evaluate the pH responsiveness of the TpPa-based membranes, we measured conductance as a function of KCl concentration at pH 3, 5, 9.5, and 11.5 [Supplementary Figures 3-6]. At each pH, all four membranes exhibit the same qualitative behavior seen at pH 7: conductance decreases approximately linearly with dilution at high salt concentrations and transitions to a much weaker concentration dependence at low salt concentrations, indicating that the surface-charge-governed transport regime persists throughout the pH range. However, the magnitude of conductance varies markedly with pH. The low-concentration plateau (10^{-7}-10^{-5} M) conductance for the four membranes at pH 11.5 (*ca.* 54-96 μS, Supplementary Figure 3H) and at pH 3 (*ca.* 35-64 μS, Supplementary Figure 4H) is 19- to 114-fold higher than the corresponding values at pH 7 (*ca.* 0.47-2.49 μS, Figure 2B). The transition between the two concentration regimes is less pronounced at extreme pH because the increased concentration and high mobility of H^+ or OH^- raise the low-concentration conductance, reducing the contrast with the high-concentration regime.

The intermediate pH values reveal the influence of functional-group chemistry. At pH 5, the conductance of all four membranes decreases substantially relative to pH 3 due to the decreased H^+ concentration. The four membranes converge to a narrow range of 2.2-4.3 μS at 10^{-5} M [Supplementary Figure 5H and Supplementary Table 3]. For TpPa-COOH, pH 5 is close to the carboxyl pKa, and this membrane exhibits lower conductance than TpPa-OH below 10^{-4} M. At pH 9.5, near the phenol pKa (≈ 9-10), the conductance

trend follows a different pattern [Supplementary Figure 6H]. TpPa-COOH exhibits higher conductance than TpPa-OH at concentrations above approximately 10^{-3} M, whereas TpPa-OH surpasses TpPa-COOH below 10^{-4} M. This reversal reflects the progressive deprotonation of the phenol groups in TpPa-OH, which generates an effective surface charge that becomes increasingly important as the salt concentration decreases.

To further quantitatively compare pH-dependent behavior across membranes, we focused on 10^{-6} M KCl, where the Debye length (about 300 nm) far exceeds the channel dimensions. This concentration falls well within the surface-charge-governed regime for all membranes (below 10^{-5} M), yet remains sufficiently above the extreme dilution limit (10^{-7} M) where hydronium contributions begin to complicate the interpretation. As shown in Figure 3A and Supplementary Table 4, all membranes display a U-shaped pH dependence: high conductance is observed at both acidic (pH 3) and alkaline (pH 11.5) extremes, with a minimum near neutral pH. The depth of the conductance minimum and the steepness of the pH response vary among membranes. TpPa-SO_3H maintains the highest conductance at all pH values, including the minimum at pH 7 (0.89 ± 0.09 μS). TpPa-COOH exhibits the most pronounced pH response, with a sharp decrease from 54.4 ± 3.56 to 2.2 ± 0.18 μS between pH 3 and pH 5, coinciding with the carboxyl pKa (≈ 4.5). Its conductance at pH 7 (0.48 ± 0.04 μS) is the lowest among all membranes, lower than that of unmodified TpPa (0.60 ± 0.05 μS). At pH ≥ 5, TpPa-COOH has lower conductance than TpPa-OH. TpPa-OH demonstrates a conductance minimum at pH 7 (0.62 ± 0.12 μS) slightly higher than that of TpPa-COOH, and a steep alkaline rise that coincides with the phenol pKa (≈ 9-10).

The ON/OFF ratios are defined as the conductance at pH 3 or 11.5 divided by that at pH 7 to quantify the pH-gating amplitude [Supplementary Table 4]. TpPa-SO_3H shows the smallest ratios (70 acidic-neutral, 79 alkaline-neutral) because of its high baseline conductance at pH 7, despite maintaining the highest absolute conductance at both extremes. TpPa-COOH displays the largest acidic-to-neutral ratio (113), consistent with its sharp decrease from pH 3 to pH 7, and the highest alkaline-to-neutral ratio (114) due to its lowest conductance at pH 7. TpPa-OH exhibits an alkaline-to-neutral ratio of 101, indicating the onset of phenolate deprotonation above pH 9. The unmodified TpPa also presents notable ratios (71 acidic-neutral, 98 alkaline-neutral), which can be attributed to the framework's intrinsic pH response and non-specific adsorption. These values are comparable to those reported for the COF-DT membrane (~ 100)[13]. To assess reversibility, we cycled the solution pH between 3 and 7, and separately between 7 and 11.5, while monitoring conductance at 10^{-6} M [Figure 3B and C]. All four membranes recover their initial conductance after each cycle, with no measurable drift over four cycles, consistent with reversible protonation/deprotonation of framework sites and functional groups, as well as reversible ion adsorption/desorption for unmodified TpPa, rather than irreversible structural changes to the COF framework.

Mechanistic origin of pH-gating ion transport

To understand the origin of these pH-dependent conductance differences, we examined the surface charge densities (σ) derived from the ζ potential measurements [Figure 1H] as a function of pH [Figure 3D and Supplementary Table 5]. For TpPa-SO_3H, the absolute value of σ increases monotonically from 0.86 mC m^{-2} at pH 3 to 2.31 mC m^{-2} at pH 10. TpPa-COOH and TpPa-OH show similar increases (from 0.30 to 2.02 mC m^{-2} and from 0.59 to 1.85 mC m^{-2}, respectively). TpPa is positively charged at pH 3 (+20.4 mV, σ = 1.51 mC m^{-2}) due to imine protonation, but becomes negatively charged at pH ≥ 5, with σ rising from 0.51 mC m^{-2} at pH 5 to 2.29 mC m^{-2} at pH 10. Across this pH range, however, the conductance follows a U-shaped curve rather than a monotonic trend.

The zero-current potentials at pH 7 [Figure 3E] follow the order TpPa (40.7 ± 1.33 mV) > TpPa-SO_3H (17.4 ± 2.47 mV) > TpPa-COOH (12.8 ± 1.34 mV) > TpPa-OH (4.9 ± 2.24 mV). For TpPa-R, this order correlates with σ at pH 7 (1.59, 1.56, and 1.32 mC m^{-2} for TpPa-SO_3H, TpPa-COOH, TpPa-OH, respectively), whereas

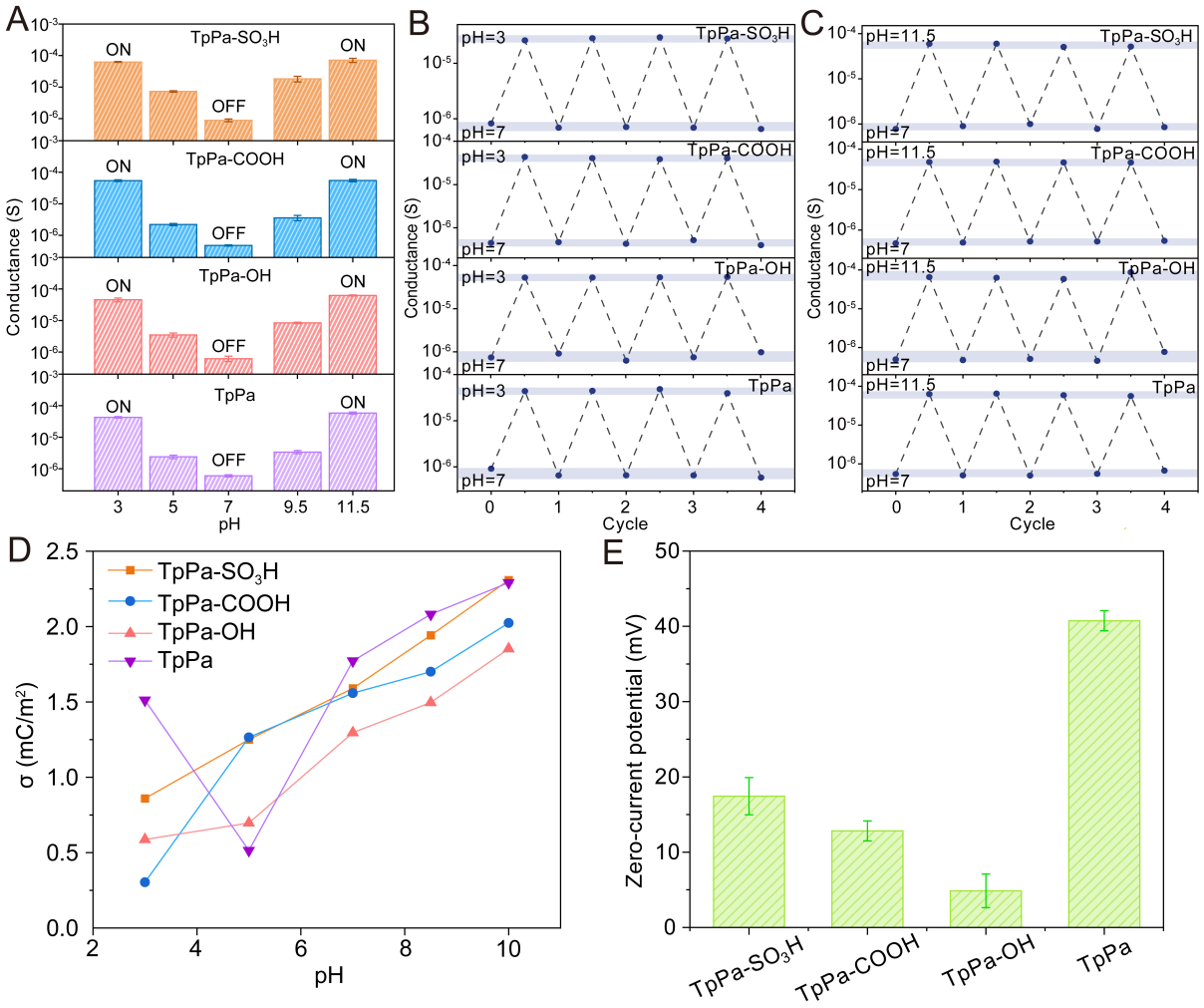


Figure 3. pH-gated ion transport in TpPa-based COF membranes. (A) Conductance at 10^{-6} M KCl as a function of pH for the four membranes. Reversible conductance switching (B) between pH 7 and pH 3, and (C) between pH 7 and pH 11.5 at 10^{-6} M KCl. Shaded areas indicate the fluctuation range over consecutive cycles; (D) Apparent surface charge density (σ) calculated from ζ potential measurements as a function of pH; (E) Zero-current potential of the four COF membranes at pH 7. Error bars in (A) and (E) represent the standard deviation obtained from three independent measurements for each sample and condition. COF: Covalent organic framework.

TpPa exhibits a slightly higher σ (1.77 mC m^{-2}) but a much larger zero-current potential. This deviation indicates a different nature of the surface charge: covalently tethered charges in TpPa-R are symmetrically distributed, giving small Donnan potential differences, while non-specific OH^- adsorption in TpPa is asymmetric and produces a larger potential difference. The low zero-current potential of TpPa-OH indicates the most symmetric charge distribution across the membrane under symmetric conditions. Together with the U-shaped conductance profile, these results indicate that σ alone is insufficient to describe ion transport. A more appropriate descriptor is effective surface charge density (σ_{eff}), defined as the fraction of the apparent charge that participates in counterion enrichment. For the four TpPa-based membranes, σ_{eff} depends on two factors. The pKa of each functional group sets the pH at which surface charge appears. The chemical environment of that charge, including its hydration, spatial localization, and covalent fixation, then determines how effectively it enriches counterions[34,35].

With σ_{eff} as the central parameter, the pH-dependent behavior of the four membranes can be understood as follows. As illustrated in Figure 4, at low pH (3-5), the abundance and high mobility of H^+ provide a high background conductance to all four membranes[36]. The actual conductance of each membrane, however,

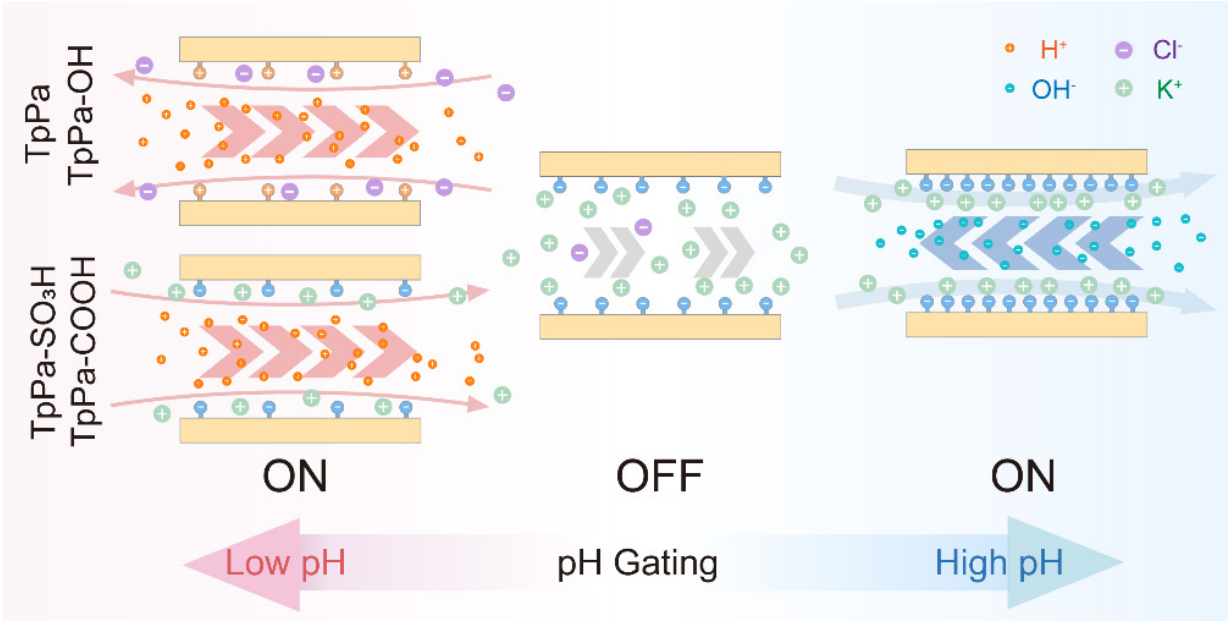


Figure 4. Schematic illustration of the ion transport mechanism in TpPa-R membrane nanochannels under different pH conditions.

depends on how effectively its pore surface enriches counterions. TpPa-SO_3H with fully deprotonated sulfonate groups (pKa < 0) remains negatively charged and enriches both K^+ and H^+, giving the highest σ_{eff} and conductance. The nearly neutral TpPa-COOH accumulates cations weakly, resulting in an intermediate σ_{eff} and conductance. In contrast, the protonated TpPa-OH and TpPa with positively charged pores partially enrich Cl^- while repelling cations, leading to lower σ_{eff} and conductance. At high pH (9.5-11.5), the bulk OH^- with high mobility also provides a high background conductance. Deprotonation of pH-responsive groups and framework sites renders all membranes negatively charged, enhancing σ_{eff} and conductance. The differences in high-pH conductance reflect differences in σ_{eff} for all membranes at the same bulk OH^- concentration. TpPa-SO_3H maintains the highest σ_{eff}, while TpPa-OH surpasses TpPa-COOH, and TpPa exhibits intermediate σ_{eff}. These observations indicate that σ_{eff} remains effective even when bulk H^+ or OH^- concentrations are high. The "ON" state at extreme pH therefore results from the combined effects of bulk H^+ or OH^- conduction and pore-surface charge regulation.

Under neutral pH conditions, H^+ and OH^- contributions are minimal, and σ_{eff} governs transport. TpPa-SO_3H shows the shallowest minimum at pH 7, consistent with its fully dissociated sulfonate groups, which have a highly localized charge and minimal hydration screening. TpPa-COOH exhibits the deepest minimum, lower than that of TpPa-OH, despite its higher σ at pH 7. This inversion can be attributed to the strong hydration shell of the carboxylate groups, which partially screens the fixed charges through dielectric shielding, reducing σ_{eff} for counterion enrichment[27]. The same hydration screening also accounts for the lower σ_{eff} of TpPa-COOH relative to TpPa-OH at high pH. TpPa, whose charge arises from physically adsorbed OH^-, exhibits a minimum consistent with its low σ_{eff}.

The pH response of the four membranes is therefore governed by the interplay between σ_{eff} and the high-mobility carriers (H^+ and OH^-). The relative weight of these two contributions varies with functional group and pH, leading to the different response amplitudes observed.

pH-responsive membrane potential and biomimetic switching

The pH-gradient membrane potential experiment parallels the electrophysiological behavior of biological membranes, which use surface charges and ion channels to generate membrane potentials and regulate

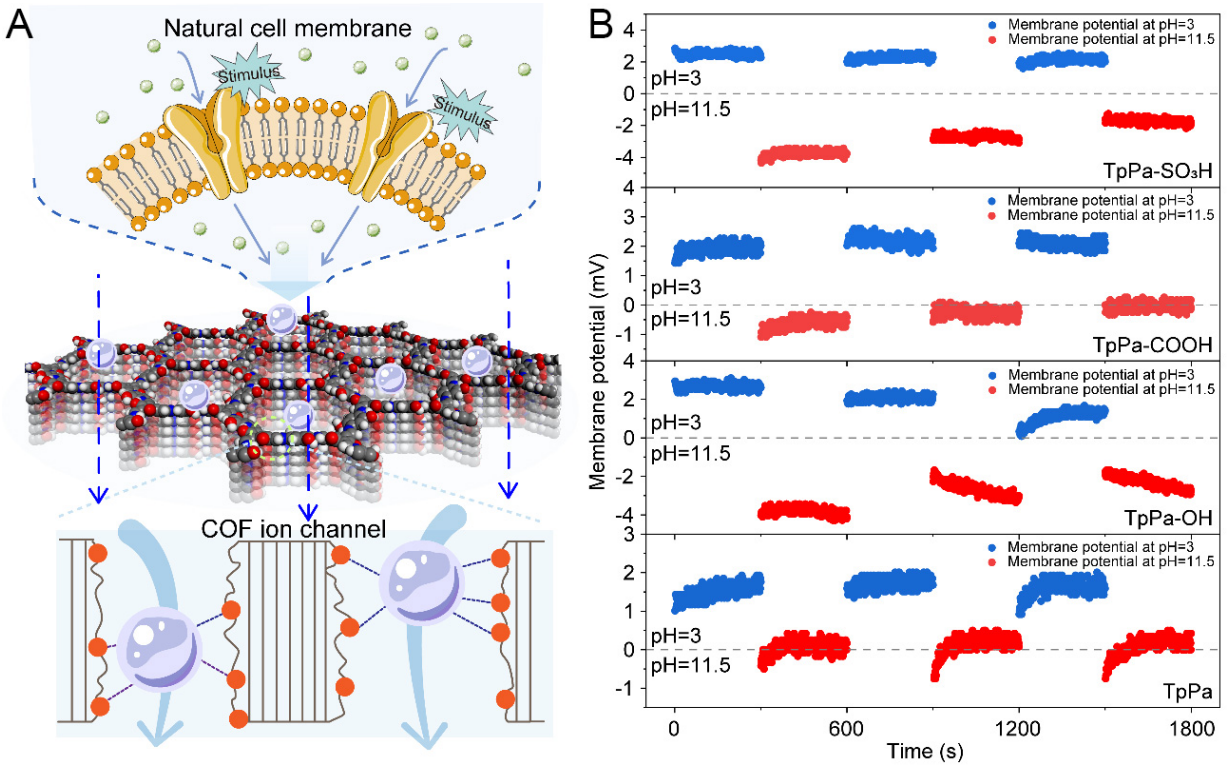


Figure 5. (A) Schematic illustration of the bioinspired design of TpPa-R COF membranes for mimicking pH-gated biological ion channels. (B) Membrane potential responses of TpPa-R and TpPa membranes under asymmetric pH conditions, with one side switched between pH 3 and pH 11.5 while the other remained at pH 7. COF: Covalent organic framework.

selectivity. COF membranes, with pH-responsive surfaces and well-defined nanochannels, offer a suitable biomimetic platform [Figure 5A]. We measured the pH-responsive potentials of TpPa-based membranes under asymmetric pH gradients [Figure 5B]. All four membranes generate pH-responsive membrane potentials: positive under pH 7|3 and negative under pH 7|11.5 (TpPa near 0 mV). This polarity reversal indicates the pH-induced change in the internal electric field. When one side of the membrane is cycled between acidic and alkaline conditions, the field direction reverses, altering the preferential migration direction of cations and anions and thereby reversing the potential polarity.

The four TpPa-based membranes exhibit distinct membrane potentials, indicating differences in the pH-responsive behavior of their functional groups. Under acidic gradients (pH 7|3), the membrane potentials are +2.3, +2.6, +2.1, and +1.6 mV for TpPa-SO_3H, TpPa-OH, TpPa-COOH, and TpPa, respectively. For TpPa-SO_3H, the high and stable potential originates from the high σ_{eff} of its negative sulfonate groups, which promotes cation-selective migration. TpPa-OH exhibits the highest potential, likely due to the enhanced proton transport through hydrogen-bond networks formed by its phenolic hydroxyl groups[37,38]. The lower potentials of TpPa-COOH and TpPa probably reflect hydration screening of the carboxylate groups in the former, and the absence of strongly ionizable groups in the latter. Under alkaline gradients (pH 7|11.5), TpPa-SO_3H and TpPa-OH both give -3.8 mV, whereas TpPa-COOH gives -0.3 mV and TpPa remains near 0 mV. For TpPa-SO_3H and TpPa-OH, the sulfonate and phenolate groups remain fully deprotonated, maintaining high effective negative charge and cation selectivity. TpPa-COOH loses most of its membrane potential, also likely attributed to hydration screening effect, while TpPa relies only on intrinsic framework charges, giving a near-zero membrane potential.

With repeated pH-switching cycles, the membrane potentials decay toward 0 V, most markedly for TpPa-COOH and TpPa-OH. This decay is likely attributed to (i) transient ion trapping within the nanochannels

via strong electrostatic interactions with deprotonated groups, and (ii) incomplete recovery of protonation/deprotonation states, particularly for -OH and -COOH groups with higher pKa values[20,23]. These observations suggest that pulsed pH switching or periodic regeneration may improve cycling stability. This pH-switchable ion selectivity distinguishes these membranes from conventional pH-gating systems that modulate conductance magnitude, and makes them promising for biomimetic iontronic applications requiring directional ion control.

CONCLUSIONS

In summary, we have demonstrated chemically programmable pH-gated ion transport in TpPa-based COF membranes with oxygen-containing groups (-SO_3H, -COOH, and -OH). The pH-dependent conductance followed a common U-shaped profile, with maxima at acidic and alkaline extremes and a minimum near neutral pH. Surface-charge-governed transport remained operative across the entire pH range, dominating at low ionic strength and neutral pH while contributing alongside high-mobility H^+ and OH^- at the extremes. The σ_{eff}, rather than the apparent charge density from ζ potentials, governed ion transport. TpPa-SO_3H exhibited the broadest pH responsiveness and highest ion conductance due to its full dissociation and high σ_{eff}. TpPa-COOH showed lower conductance than TpPa-OH at pH ≥ 5 despite higher apparent surface charge, an inversion caused by hydration screening that reduced σ_{eff}. Conversely, deprotonation of the phenol groups of TpPa-OH enhanced σ_{eff} and conductance. The pKa of each group set the pH window of the conductance minimum, while σ_{eff} dictated its depth, enabling reversible ON/OFF ratios exceeding 110 for TpPa-COOH. Under asymmetric pH gradients, the membrane potential polarity reversed, indicating a reversal in the preferred direction of ion transport and distinguishing this system from conventional pH-gating platforms that primarily modulate conductance magnitude. These results establish a molecular design principle for smart nanofluidic membranes, where functional group selection programs both the pH response window and switching amplitude, offering a versatile platform for programmable pH-responsive iontronic systems.

DECLARATIONS

Acknowledgments

We thank Professor Xiangyu Kong and Dr. Weiwen Xin from the Institute of Physical and Chemical Research, Chinese Academy of Sciences, for their technical guidance. We also extend our gratitude to the Large-scale Instrumentation Sharing Platform at China University of Geosciences (Beijing) for its support.

Authors' contributions

Led the project and conceived the idea: Sun, B.

Made substantial contributions to the conception and design of the study and performed data analysis and interpretation: Li, P.; Zhang, J.; Luo, L.

Carried out the supplementary experiments: Yang, M.; Xia, A.; Niu, Y.

Performed draft revision and provided administrative, technical, and material support: Sun, B.; Li, P.

Contributed to the discussions of the manuscript: Zhang, J.; Yang, M.; Xia, A.; Niu, Y.

Availability of data and materials

The original contributions presented in this study are included in the article/Supplementary Materials. Further inquiries can be directed to the corresponding author.

Financial support and sponsorship

None.

AI and AI-assisted tools statement

During the preparation of this manuscript, the AI tool DeepSeek (version V4-Flash, released 2026-07-31) was used solely for language editing. The tool did not influence the study design, data collection, analysis, interpretation, or the scientific content of the work. All authors take full responsibility for the accuracy,

integrity, and final content of the manuscript.

Conflicts of interest

All authors declared that there are no conflicts of interest.

Ethical approval and consent to participate

Not applicable.

Consent for publication

Not applicable.

Copyright

© The Author(s) 2026.

Supplementary Materials

Supplementary Materials

REFERENCES

1. Hou, X.; Guo, W.; Jiang, L. Biomimetic smart nanopores and nanochannels. *Chem. Soc. Rev.* **2011**, *40*, 2385-401. DOI
2. Yu, L.; Li, X.; Luo, C.; et al. Bioinspired nanofluidic iontronics for brain-like computing. *Nano. Res.* **2024**, *17*, 503-14. DOI
3. Zhang, Z.; Wen, L.; Jiang, L. Bioinspired smart asymmetric nanochannel membranes. *Chem. Soc. Rev.* **2018**, *47*, 322-56. DOI
4. Zhou, S.; Ai, F.; Song, Z.; et al. TASK2-inspired pH-gating polymeric nanochannels with multiple interconvertible permeability states by synergistic regulation of conformation and charge. *Angew. Chem. Int. Ed. Engl.* **2025**, *64*, e202512145. DOI
5. Lopez, L. G.; Nap, R. J. Highly sensitive gating in pH-responsive nanochannels as a result of ionic bridging and nanoconfinement. *Phys. Chem. Chem. Phys.* **2018**, *20*, 16657-65. DOI PubMed
6. Huang, W. L.; Wang, X. D.; Ao, Y. F.; Wang, Q. Q.; Wang, D. X. An artificial single molecular channel showing high chloride transport selectivity and pH-responsive conductance. *Angew. Chem. Int. Ed. Engl.* **2023**, *62*, e202302198. DOI PubMed
7. Su, Y.; Hung, W.; Fauziah, A. R.; Siwy, Z. S.; Yeh, L. A pH gradient induced rectification inversion in asymmetric nanochannels leads to remarkably improved osmotic power. *Chem. Eng. J.* **2023**, *456*, 141064. DOI
8. Yeh, L. H.; Zhang, M.; Qian, S. Ion transport in a pH-regulated nanopore. *Anal. Chem.* **2013**, *85*, 7527-34. DOI
9. Zhao, C.; Hou, J.; Hill, M.; Freeman, B.; Wang, H.; Zhang, H. Enhanced gating effects in responsive sub-nanofluidic ion channels. *Acc. Mater. Res.* **2023**, *4*, 786-97. DOI
10. Zare, R. N. Interfacial chemistry as a foundation for future iontronics. *Iontronics* **2026**, *2*, 21. DOI
11. Sun, Q.; Dou, P.; Du, J.; et al. Biomimetic KcsA channels enabled by 1D MOF-in-2D COF. *Nat. Commun.* **2025**, *16*, 9099. DOI PubMed PMC
12. Malla, J. A.; Fenton, K. J.; Bellamkonda, A.; Fidler, S. I.; Wallace, M. I.; McTernan, C. T. Triply responsive control of ion transport with an artificial channel creates a switchable AND to OR logic gate. *Angew. Chem. Int. Ed. Engl.* **2026**, *65*, e17444. DOI
13. Cao, L.; Liu, X.; Shinde, D. B.; et al. Oriented two-dimensional covalent organic framework membranes with high ion flux and smart gating nanofluidic transport. *Angew. Chem. Int. Ed. Engl.* **2022**, *61*, e202113141. DOI
14. Guo, Q.; Yi, J.; Lv, H.; Lai, Z.; Sun, Q. Covalent organic framework membranes for ion separation and ion-driven energy conversion. *Chem. Soc. Rev.* **2026**, *55*, 5728-75. DOI
15. Ren, L.; Song, J.; Zhang, N.; Guo, Y.; Belzile, N.; Deng, T. Crown ether rotaxane-induced construction of COF membranes with recognition channels for high-efficiency ion sieving. *Angew. Chem. Int. Ed. Engl.* **2026**, *65*, e25413. DOI PubMed
16. Jiang, G.; Zou, W.; Ou, Z.; et al. Precise regulation of intra-nanopore charge microenvironment in covalent organic frameworks for efficient monovalent cation transport. *Angew. Chem. Int. Ed. Engl.* **2025**, *64*, e202420333. DOI
17. Lai, Z.; Lv, H.; Guo, Q.; Sun, Q. Design principles of permselective nanochannels for iontronic applications in the energy-water nexus: taking covalent organic frameworks as an example. *Small* **2026**, *22*, e10616. DOI
18. Lee, W.; Li, H.; Du, Z.; Feng, D. Ion transport mechanisms in covalent organic frameworks: implications for technology. *Chem. Soc. Rev.* **2024**, *53*, 8182-201. DOI
19. You, X.; Cao, L.; Liu, Y.; et al. Charged nanochannels in covalent organic framework membranes enabling efficient ion exclusion. *ACS. Nano.* **2022**, *16*, 11781-91. DOI
20. Xu, R.; Xu, X.; Alowasheeir, A.; Yamauchi, Y.; Jiang, D. Carboxyl-functionalized covalent organic framework for high-performance capacitive deionization. *Bull. Chem. Soc. Jpn.* **2025**, *98*, uoaf053. DOI

21. Wei, X.; Liu, Y.; Zhao, F.; et al. Covalent organic framework membrane with hourglass-shaped nanochannels for ultrafast desalination. *Nat. Commun.* **2025**, *16*, 8125. DOI PubMed PMC
22. Wu, Z.; Wang, M.; Liu, X.; et al. Spatial size manipulation of 1D/2D channels in covalent organic framework membranes through dopamine chemistry for ion separations. *Adv. Funct. Mater.* **2025**, *35*, 2416228. DOI
23. Cao, L.; Chen, I. C.; Li, Z.; et al. Switchable Na^+ and K^+ selectivity in an amino acid functionalized 2D covalent organic framework membrane. *Nat. Commun.* **2022**, *13*, 7894. DOI PubMed PMC
24. Zhao, W.; Yang, J.; Wang, Z.; et al. Reversible bond dynamics enable crystallinity-healed COF membranes for selective ion transport. *Small* **2026**, *22*, e13711. DOI PubMed PMC
25. Xue, Y.; Yuan, X.; Chen, C.; et al. Cross-layer alternating paired charge distribution to boost proton conductivity of COF lamellar membrane. *J. Membr. Sci.* **2025**, *717*, 123556. DOI
26. Liu, X.; Wang, J.; Shang, Y.; Yavuz, C. T.; Khashab, N. M. Ionic covalent organic framework-based membranes for selective and highly permeable molecular sieving. *J. Am. Chem. Soc.* **2024**, *146*, 2313-8. DOI PubMed PMC
27. Wang, H.; Zhai, Y.; Li, Y.; et al. Covalent organic framework membranes for efficient separation of monovalent cations. *Nat. Commun.* **2022**, *13*, 7123. DOI PubMed PMC
28. Wang, X.; Shi, X.; Zhang, Z.; Yin, C.; Zhang, Z.; Wang, Y. Ion-pairing design of covalent organic framework membranes for separation and controlled release of pharmaceuticals. *J. Membr. Sci.* **2024**, *693*, 122347. DOI
29. Dong, P.; Cheng, T.; Zhang, J.; et al. Fabrication of an organic/inorganic hybrid TpPa-1-COF/$ZnIn_2S_4$ S-scheme heterojunction for boosted photocatalytic hydrogen production. *ACS. Appl. Energy. Mater.* **2023**, *6*, 1103-15. DOI
30. Cao, J.; Dong, X.; Pang, X.; et al. Anionic COF-cationic polymer hybrid anion-exchange membranes with enhanced hydroxide conductivity. *Chem. Eng. J.* **2025**, *525*, 170258. DOI
31. Kandambeth, S.; Mallick, A.; Lukose, B.; Mane, M. V.; Heine, T.; Banerjee, R. Construction of crystalline 2D covalent organic frameworks with remarkable chemical (acid/base) stability via a combined reversible and irreversible route. *J. Am. Chem. Soc.* **2012**, *134*, 19524-7. DOI
32. Li, X.; Zuo, P.; Ge, X.; Yang, Z.; Xu, T. Constructing new-generation ion exchange membranes under confinement regime. *Natl. Sci. Rev.* **2025**, *12*, nwae439. DOI PubMed PMC
33. Zhu, T.; Kong, Y.; Lyu, B.; et al. 3D covalent organic framework membrane with fast and selective ion transport. *Nat. Commun.* **2023**, *14*, 5926. DOI PubMed PMC
34. Cheng, P.; Chen, T.; Liu, T.; et al. Covalent/metal-organic framework membranes with tailored pore functionality for accurate ion separation. *Chem. Sci.* **2025**, *16*, 22900-32. DOI PubMed PMC
35. Li, X.; Zhang, Y. Microenvironments engineering on covalent organic framework nanofluidics for high flux and ion selectivity. *Iontronics* **2026**, *2*, 29. DOI
36. Zhang, Z.; Qiao, Z.; Yang, D.; Shi, L. Deciphering the role of sulfonated side-chain length in modulating proton transport in TpBd-COFs. *J. Mater. Chem. A.* **2026**, *14*, 29232-42. DOI
37. Zong, L.; Tao, S.; Xu, X.; Feng, Y.; Wen, F.; Huang, N. Atomic engineering in covalent organic frameworks for high-performance proton conduction. *J. Mater. Chem. A.* **2025**, *13*, 19355-61. DOI
38. Yang, Y.; Zhang, P.; Hao, L.; Cheng, P.; Chen, Y.; Zhang, Z. Grotthuss proton-conductive covalent organic frameworks for efficient proton pseudocapacitors. *Angew. Chem. Int. Ed. Engl.* **2021**, *60*, 21838-45. DOI

Disclaimer/Publisher's Note: All statements, opinions, and data contained in this publication are solely those of the individual author(s) and contributor(s) and do not necessarily reflect those of OAE and/or the editor(s). OAE and/or the editor(s) disclaim any responsibility for harm to persons or property resulting from the use of any ideas, methods, instructions, or products mentioned in the content.

© The Author(s) 2026. Open Access This article is licensed under a Creative Commons Attribution 4.0 International License (https://creativecommons.org/licenses/by/4.0/), which permits unrestricted use, sharing, adaptation, distribution and reproduction in any medium or format, for any purpose, even commercially, as long as you give appropriate credit to the original author(s) and the source, provide a link to the Creative Commons license, and indicate if changes were made.